American Mineralogist, Volume 110, pages 1877–1885, 2025

Synthesis of zircon-hafnon to determine oxygen isotope matrix effects in secondary ionization mass spectrometry

Axel K. Schmitt[1,2,*,†], Leonid Aranovich[3,‡], and Ilya Bindeman[4,5,§]

[1]John de Laeter Centre, Curtin University, Kent Street, Bentley, Western Australia 6102, Australia
[2]Institut für Geowissenschaften, Heidelberg University, Im Neuenheimer Feld 234-236, 69120 Heidelberg, Germany
[3]Institute of Geology of Ore Deposits, Petrography, Mineralogy, and Geochemistry of the Russian Academy of Sciences, Staromonetnyi per. 35, Moscow 119017, Russia
[4]Department of Earth Sciences, University of Oregon, 110A Cascade Hall, 1272 University of Oregon, Eugene, Oregon 97403-1205, U.S.A.
[5]Institut für Geowissenschaften, Johannes Gutenberg-Universität, J.-J.-Becher-Weg 21, 55128 Mainz, Germany

Abstract

Secondary ionization mass spectrometry (SIMS) is a powerful tool for precise, correlative actinide decay chain dating, trace element analysis, and stable isotope analysis of accessory minerals, offering unrivaled nanogram-scale sampling. Matrix-matched reference materials are a prerequisite for accurate quantification of isotopic compositions by SIMS. For rock-forming and accessory minerals showing partial or complete solid solution, elaborate correction schemes are required for SIMS isotope analysis. Natural zircon ($ZrSiO_4$), often with a nearly stoichiometric end-member composition, has traditionally required less attention to matrix matching between reference materials and unknowns. However, with increasing analytical precision afforded by multi-collection SIMS instrumentation, it is important to experimentally verify this assumption and define its limitations. Here, we focus on Hf in zircon (Zrn), which is isomorphous with hafnon (Hfn), and the fourth most abundant element in natural zircon. Two end-members in the Zrn-Hfn solid solution and three intermediate compositions were synthesized in a MoO_3-Li_2MoO_4 flux. Oxygen isotopic compositions of synthetic Zrn-Hfn crystals were determined at the milligram scale by laser fluorination isotope ratio mass spectrometry, and at lateral and depth resolutions of ~15 and ~1 μm, respectively, by SIMS. Despite a detected ~1–3‰ isotopic heterogeneity in flux-grown Zrn-Hfn, a strong correlation between instrumental mass fractionation and the zirconium number Zr# % (atomic Zr/[Zr+Hf] × 100) was observed (Pearson correlation coefficient r = 0.9958), with ~8.8‰ variation in $\delta^{18}O$ across the compositional range. For most natural zircon, including common reference materials, the interpolated matrix effect is smaller than typical analytical uncertainties for individual SIMS spots (~0.1‰). Only $\delta^{18}O$ analysis of Hf-rich pegmatite zircon by SIMS requires significant (up to ~3‰) matrix corrections. In such cases, the matrix effect on instrumental mass fractionation can be linearly interpolated between a common low-Hf zircon reference and the synthetic Hfn end-member to within ~0.1–0.2‰ uncertainty.

Keywords: Accessory minerals, stable isotopes, mass spectrometry, solid solution, flux growth

Introduction

A ubiquitous accessory mineral in igneous, metamorphic, and sedimentary rocks, zircon is universally important in geological and planetary sciences as a carrier of geochronological and geochemical information. All stoichiometric components in zircon (Zr, Si, and O) have multiple stable isotopes which are routinely analyzed, often with spatially selective microanalytical instrumentation including secondary ionization mass spectrometry (SIMS) and, for Zr and Si, laser ablation with inductively coupled plasma mass spectrometry (LA-ICP-MS) to constrain conditions of its formation and preservation (e.g., Liebmann et al. 2023; Trail et al. 2018; Tompkins et al. 2020). The next most abundant element in zircon is Hf, which is a geochemical twin of Zr and in chondrite 34.2 times less abundant by mass than Zr in chondrites (Weyer et al. 2002). Because of its geochemical similarity with Zr as controlled by ionic size and charge (Bau 1996), Hf exceptionally rarely forms its own minerals, but instead commonly substitutes for Zr. For the same reason, its late discovery in 1923 in zircon concentrates happened long after Mendeleev had predicted its existence in 1869, based on the order of the periodic table. Natural zircon thus forms a solid solution series between the end-members zircon (Zrn) and hafnon (Hfn), although neither is recognized in nature as a pure phase.

Zircon oxygen isotopic compositions are commonly expressed as $\delta^{18}O$ relative to Vienna Standard Mean Ocean Water (V-SMOW; $^{18}O/^{16}O = 0.0020052$) (Baertschi 1976). On this scale, zircon crystallized from mantle-derived melts falls into a narrow range at 5.3 ± 0.3‰ (Valley 2003). Substantially higher or lower $\delta^{18}O$ values in zircon commonly indicate

* Corresponding author E-mail: axel.schmitt@curtin.edu.au Orcid https://orcid.org/0000-0002-9029-4211

‡ Orcid https://orcid.org/0000-0002-8229-9469
§ Orcid https://orcid.org/0000-0003-2778-9083

0003-004X/25/0012–1877$05.00/DOI: https://doi.org/10.2138/am-2025-9886

oxygen isotopic exchange of water with minerals in the protoliths of zircon-crystallizing melts, either at low temperature (leading to elevated $\delta^{18}O$ in pelites) (e.g., Lackey et al. 2005) or high temperature (producing low-$\delta^{18}O$ signatures in hydrothermally altered rocks and their igneous or metamorphic products) (e.g., Yui et al. 1997; Wotzlaw et al. 2012), respectively. Moreover, oxygen isotopes in zircon can reveal isotopic exchange with fluids in metamict zircon, although non-metamict zircon shows remarkable stability in high-temperature fluids (e.g., Booth et al. 2005; Liebmann et al. 2021). For $\delta^{18}O$ determined by SIMS, data are often combined with Hf isotopic analysis by LA-ICP-MS. In the Hf-isotopic system, radioactive decay of ^{176}Lu to ^{176}Hf over time has produced isotopic signatures in crustal and mantle reservoirs with distinct compositions relative to bulk Earth (expressed as εHf relative to the chondritic uniform reservoir). In combination, the isotope systems form a powerful means of tracking planetary-scale differentiation and lithosphere-scale rock cycles throughout geological time (e.g., Hawkesworth and Kemp 2006).

SIMS is widely used to determine oxygen isotopic compositions in minerals due to the high spatial resolution (at typically ~10–15 μm lateral and sub-μm depth dimensions) and rapidness (ca. 3 min per analysis spot) it affords. For zircon, $\delta^{18}O$ can also be directly correlated with U-Th-Pb ages, trace element abundances, and other radiogenic or stable isotope systems. Critical for accurate SIMS analysis is the availability of reference minerals that compositionally match unknowns. These must be analyzed under analytical conditions that are maintained as close as possible to those for the unknowns to yield an instrumental mass fractionation factor (IMF) α:

$$\alpha = \frac{(18/16)_{SIMS}}{(18/16)_{LF-IRMS}} \quad (1)$$

In this equation, the numerator expresses the intensity ratios for $^{18}O^-$ and $^{16}O^-$ SIMS signals (corrected for detector baseline and yield) and the denominator the "known" composition, typically based on precise laser fluorination isotope ratio mass spectrometry (LF-IRMS) analyses of well-characterized and homogeneous zircon reference materials [Table 1 after Liebmann et al. (2023)]. The "true" value of the matrix-matched unknown is then determined as:

$$(18/16)_{Unknown} = \frac{(18/16)_{SIMS}}{\alpha} \quad (2)$$

Compositional variability is known to affect the IMF, and therefore, an extensive body of literature has aimed to determine correction procedures for SIMS oxygen isotopic analysis of natural minerals exhibiting solid solution. This includes rock-forming and accessory mineral groups such as carbonates (e.g., Fayek et al. 2001; Śliwiński et al. 2016), garnet (e.g., Page et al. 2010; Ickert and Stern 2013), plagioclase (e.g., Coogan et al. 2007), olivine (e.g., Isa et al. 2017), and tourmaline (e.g., Whattam et al. 2022). For the Zrn-Hfn solid solution, however, IMF for $^{18}O/^{16}O$ has only been quantified for high-energy secondary ion detection in a small-geometry SIMS instrument, at low precision compared to modern methods, and over a limited compositional range (Eiler et al. 1997). Because modern SIMS stable isotopic analysis applies multi-collection detection without energy offsets in large-geometry instruments with increasing analytical precision, it is timely to re-address the potential impact of Zrn-Hfn substitution for SIMS $^{18}O/^{16}O$ analysis. For this, we synthesized crystals with five compositions between the Zrn-Hfn end-members, characterized them for major and trace elements as well as oxygen isotopic compositions, and compared their IMF values to a commonly used natural zircon reference material with low Hf abundance (91500) (Wiedenbeck et al. 2004).

Table 1. Compiled oxygen isotopic compositions and Hf concentrations of standard zircon reference materials

ID	$\delta^{18}O$ ‰	Reference	Hf[c] μg/g	Reference
91500[a]	9.86(22)	Wiedenbeck et al. (2004)	5895(325)	Wiedenbeck et al. (1995)
AS3[a]	5.34(6)	Trail et al. (2007); Ávila et al. (2020)	10176(933)[d]	Black et al. (2004)
BR231[a]	9.81(8)	Valley (2003)	13021(212)	Kennedy, personal communication
CZ3[a]	15.43(42)	Cavosie et al. (2011)	12980(500)	Coble et al. (2018)
GJ1[a]	6.14(36)	Xia et al. (2019)	6681(114)	Piazolo et al. (2017)
Jilin[a]	6.05(25)	Luo et al. (2021)	9135(1020)	ibid.
KIM-5[a]	5.09(12)	Valley (2003)	9851(1696)	Page et al. (2007)
KV01[b]	6.17(33)	Wei et al. (2020)	9447–13005	ibid.
LKZ-1[a]	10.72(4)	Cheong et al. (2019)	7740(620)	ibid.
M257[a]	13.93(0.22)	Nasdala et al. (2008)	10610(465)	ibid.
Mud Tank[a]	5.03(20)	Valley (2003)	9080–11900	Gain et al. (2019)
OGC (OG1)	5.86(8)	Petersson et al. (2019); Liebmann et al. (2023); Kooymans et al. (2024)	8488(1261)	Kooymans et al. (2024)
Plešovice[b]	8.11(26)	Ávila et al. (2020); Liebmann et al. (2023)	9477–14431	Sláma et al. (2008)
QGNG[b]	7.40(10)	Kooymans et al. (2024)	10055(2193)	ibid.
Qinghu[a]	5.40(20)	Li et al. (2013)	11750(1621)	ibid.
R33[a]	5.55(8)	Valley (2003); Black et al. (2004); Ávila et al. (2020)	9497(170)[d]	Black et al. (2004
SA01[a]	6.16(26)	Huang et al. (2020)	9797(1126)	ibid.
SA02[a]	6.03(28)	Huang et al. (2021)	9060(922)	ibid.
SL13[b]	11.3(2)	Ávila et al. (2020)	8910(160)	Coble et al. (2018)
Tanz[a]	6.52(28)	Hu et al. (2021)	11546(1084)	ibid.
Temora-2[a]	8.20(2)	Valley (2003); Black et al. (2004)	8310(85)[d]	Black et al. (2004)
ZS[a]	13.69(11)	Ling et al. (2022)	8544(342)	ibid.

[a] $\delta^{18}O$ values after Liebmann et al. (2023) and compiled from references provided.
[b] $\delta^{18}O$ values as averages and 2 standard deviations from references provided.
[c] Concentrations as averages or ranges based on EMPA, LA-ICP-MS, or SIMS data from reference provided; uncertainties 2 standard deviations unless indicated differently.
[d] 2 standard error of the mean.

Background: The Zircon-Hafnon Solid Solution

With identical charge (4+) and very similar ionic radii, Zr (0.84 Å) and Hf (0.83 Å) can easily replace each other in eightfold coordination with oxygen within the zircon structure, creating a continuous solid-solution series (Finch and Hanchar 2003). Unlike other solid solutions (e.g., olivine with Mg^{2+} and Fe^{2+} end-members forsterite Fo and fayalite Fa), it is uncommon to express the Hf occupancy in the mineral formula because of its relatively low abundance in natural zircon. More frequently, Hf-in-zircon abundance is stated as a weight fraction (e.g., wt% or µg/g Hf or HfO_2), or as a Zr/Hf mass ratio (e.g., Lowery Claiborne et al. 2006). Because often only Hf abundances are determined and Zr is approximated as being stoichiometrically fixed, a constant concentration of Zr of ~500 000 µg/g is assumed when calculating Zr/Hf (Lowery Claiborne et al. 2006). This approximation is reasonable for zircon with low Hf abundances, but erroneous if more Hf replaces Zr. We therefore recast weight fractions of Hf under the assumption that Zr and Hf are the only cations in the site coordinated with eight oxygen anions:

$$\frac{Zr}{Hf}(mass) = \frac{(1-x)\times M_{Zr}}{x \times M_{Hf}} \quad (3)$$

with

$$x = \frac{w_{Hf} \times M_{ZrSiO_4}}{M_{Hf} - w_{Hf} \times (M_{HfSiO_4} - M_{ZrSiO_4})} \quad (4)$$

and w_{Hf} expressing the weight fraction of Hf, and M the corresponding atomic or molecular weights (in g/mol: $M_{Zr} = 91.22$; $M_{Hf} = 178.49$; $M_{ZrSiO_4} = 183.31$; $M_{HfSiO_4} = 270.57$). Zr/Hf (mass) and Zr/Hf (mol) are readily converted, with the corresponding mole fraction X_{Hf} (mol) as:

$$\frac{Zr}{Hf}(mol) = \frac{Zr}{Hf}(mass) \times 1.96 = y \quad (5)$$

$$X_{Hf}(mol) = \frac{1}{1+y} \quad (6)$$

under the requirement that X_{Hf} and X_{Zr} sum up to unity per formula unit $(Zr,Hf)SiO_4$. Analogous to the magnesium-number (Mg#), we then define a zirconium-number in % as:

$$Zr\#\% = \frac{X_{Zr}(mol)}{X_{Zr}(mol) + X_{Hf}(mol)} \times 100 \quad (7)$$

Whereas Zr and Hf geochemically behave similarly, the slightly higher partitioning of Zr into the zircon structure relative to f leads to progressive enrichment of Hf in the residual melt from which zircon crystallized. The extremely sluggish diffusion of tetravalent cations in zircon prevents re-equilibration with the melt (Cherniak et al. 1997). Hence, even a parental melt with Zr/Hf at near chondritic values will initially crystallize zircon with super-chondritic Zr/Hf, causing a decrease in Zr/Hf in the residual melt. The next generation of zircon crystallizing upon cooling will inherit this lower Zr/Hf, again through the filter of the preferential partitioning of Zr into zircon compared to Hf. This fractionation leads to progressively lower Zr/Hf in zircon as a zircon-saturated melt cools and differentiates (Lowery Claiborne et al. 2006; Aranovich and Bortnikov 2018). Crystallization of other minerals outside of the zircon-melt boundary layer may locally enrich Hf. In extreme cases, Zr/Hf (mass) as low as ~1 is reached in pegmatitic zircon (Černý et al. 1985). In addition, variability of Hf incorporation by a factor of 2 to 3 can be kinetically controlled and mimic that of Zr isotope fractionation in zircon (e.g., Bindeman and Melnik 2022). Commonly used zircon reference materials, which are exclusively of magmatic origin, and their corresponding Hf abundances are compiled in Table 1.

Synthesis and Analytical Methods

Flux growth of zircon-hafnon

End-member zircon (Zrn) and hafnon (Hfn) as well as Zrn-Hfn solid solutions with nominal compositions of Zr# % = 95, 90, and 50 were synthesized by a flux-type method similar to that employed by Hanchar et al. (2001, 2002). Although low-temperature hydrothermal synthesis methods have been explored in the literature (Neumann et al. 2024), these reaction products are powdery, which is not ideal for SIMS analysis. A mix of 90 MoO_3 + 10 Li_2MoO_4 (wt%) was used as a flux. Reagent-grade ZrO_2, HfO_2, and amorphous silica were carefully mixed in the required stoichiometric proportions in an agate mortar with alcohol and dried at 120 °C for ca. 24 h, then mixed with the flux in proportions of 95:5 by weight for flux and reagent, respectively. About 15 g of the starting materials was loaded in 20–25 mL Pt crucibles and placed into a high temperature furnace at air. The temperature regime for synthesis was as follows: (1) increase from room temperature to 1270 °C over 250 min; (2) a dwell interval at 1270 °C for 5 h; (3) slow cooling to 982 °C over 48 h; and (4) switching off power to the furnace followed by uncontrolled cooling down to room temperature. The crystals were then extracted from the residual flux in the crucibles by washing in concentrated NH_4OH (25 wt%) and then rinsing them in distilled H_2O. Although flux inclusions were present in some synthetic crystals, they can be easily spotted under the microscope and were avoided.

Scanning electron and raman microscopy

Selected inclusion-free crystals were embedded in epoxy along with reference zircon 91500 and surrounded by fragments of NIST SRM 610 glass. After curing, the mount was sectioned using SiC and diamond abrasives to expose crystal interiors. After ultrasonic cleaning, a conductive C coating was applied, and the crystals were mapped on a Tescan Mira3 scanning electron microscope at John de Laeter Centre, Curtin University, equipped with backscattered electron (BSE) and cathodoluminescence (CL) detectors (Figs. 1a–1j). Semiquantitative chemical analyses were performed with an Oxford energy-dispersive X-ray spectrometer (EDS). After removal of the C coating, Raman spectra were acquired for selected locations on a WITec alpha300R Raman microscope using a 780 nm laser at 30 mW true-power readout, 100× objective, and 1800 grooves × mm^{-1} spectrometer grating (Fig. 1k). The spectrometer calibration was verified by detecting the 1001.4 cm^{-1} polystyrene peak (Härtel et al. 2021) at 1001.7 cm^{-1}.

Laser fluorination isotope ratio mass spectrometry (LF-IRMS)

Laser fluorination analyses in the Stable Isotope Laboratory at the University of Oregon targeted single and composite samples of synthesized Zrn-Hfn weighing between 1 and 2 mg. They were performed using BrF_5 reagent and a 10.6 µm wavelength 35 W CO_2 laser. Crystals reacted fully, and the measured yields were monitored to be close to the theoretical yield based on molecular mass. The produced O_2 was purified with a series of liquid nitrogen traps and a mercury diffusion pump (to get rid of F_2 traces), and the gas was then converted into CO_2 via a carbon-Pt rod. One sample was also analyzed as O_2 for $\Delta'^{17}O$. CO_2 and O_2 gases were expanded into the bellows on the MAT253 mass spectrometer and measured against gas calibrated on the V-SMOW scale. Silicate references run with the unknowns were in-house UOG garnet (6.52‰) and San Carlos Olivine (5.25‰, $\Delta'^{17}O = -0.051$‰). During multiple sessions, the $\delta^{18}O$ and $\Delta'^{17}O$ uncertainties on these references were ±0.07‰ and ±0.01‰, respectively (Online Materials[1] Table S1).

Secondary ionization mass spectrometry (SIMS)

Oxygen isotopes. After re-coating the mount with 80 nm Au, $^{18}O^-$ and $^{16}O^-$ were detected simultaneously in the H2 (10^{12} Ω) and L′2 (10^{10} Ω) Faraday cups (FC) on a CAMECA IMS 1300-HR[3] at Curtin University in two analytical sessions.

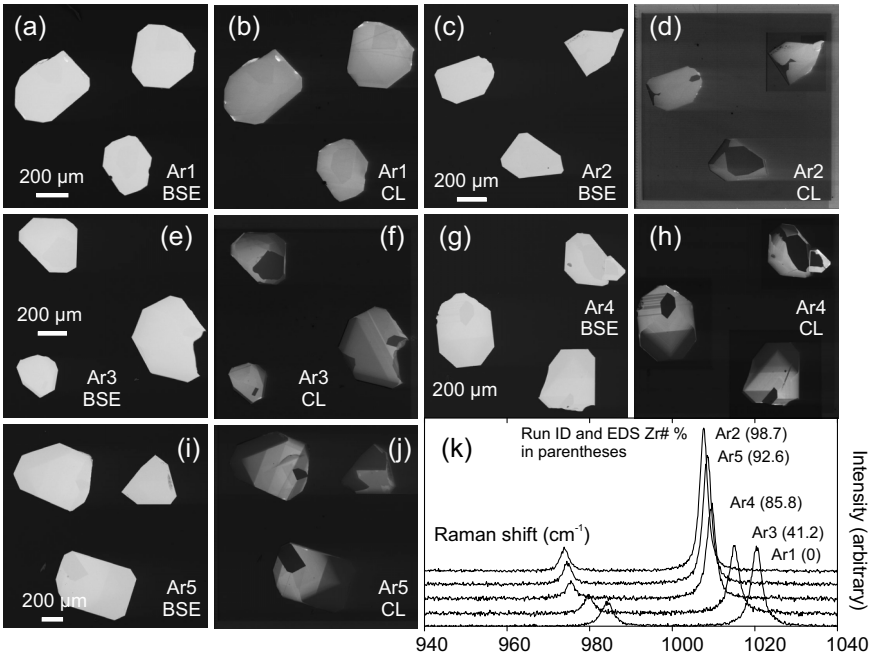

Figure 1. Backscattered electron (BSE) and cathodoluminescence (CL) overview maps of synthetic Zrn-Hfn crystals (**a**–**j**) and corresponding Raman spectra (**k**).

A ~2 nA critically focused Cs^+ beam was rastered over a 10 × 10 µm area with the mass spectrometer tuned to a transfer magnification of 60 × and a mass resolving power M/ΔM of ~2000. A total of 15 cycles with 4 s integration time each was averaged, and FC baseline intensities monitored during a 30 s pre-sputtering were subtracted from the counts using a running average of seven bracketing analyses. Faraday cup yields used for correction were determined in a gain calibration with reference voltages of 4.5 and 9 V at the beginning of the session. Blocks of four bracketing NIST SRM 610 analyses in every direction on the mount demonstrated the absence of geometry-related bias. Unknown analyses were interspersed with blocks of analyses of reference zircon 91500 (9.86‰) (Wiedenbeck et al. 2004). Selected crater volumes to determine volumetric sputter rates and useful yields (Table 2) were measured after removing the Au coat on a KLA Zeta-20 Optical Profiler at the John de Laeter Centre.

Trace elements. Selected trace elements, including P, Ti, Y, lanthanide rare earth elements (REE), Th, and U, were analyzed using an electron multiplier (EM) along with major and minor components ^{30}Si (EM), ^{90}Zr, and ^{178}Hf (both FC2 with a 10^{12} Ω feedback resistor) by peak-hopping mode using axial detectors. An ~10 nA $^{16}O^-$ beam was rastered over a 10 × 10 µm area, and secondary ions were transmitted using 80× magnification and a –100 eV energy offset at low (M/ΔM ~1000) mass resolution; only Y was analyzed at M/ΔM = 3000 due to the significant contribution of $^{178}Hf^{++}$ in Hf-doped crystals. After correction for FC baseline and EM deadtime (49 ns), trace element ratios were normalized to ^{30}Si and quantified using relative sensitivity factors (RSF) determined on NIST SRM 610 glass (Pearce et al. 1997) and verified against reference zircon 91500 (Wiedenbeck et al. 1995, 2004). Zr/Hf RSF values were directly calibrated on the 91500 reference zircon due to abundances in NIST SRM 610 being too low to be detected by the FC.

Results

Textural, compositional, and oxygen isotopic properties of synthetic Zrn-Hfn

Flux synthesis with different mixtures of ZrO_2 and HfO_2 in the starting materials produced millimeter-sized euhedral crystals with short prismatic faces and well-developed bipyramids. Interiors exhibit coarse zonation that is weakly detectable in BSE, but sometimes with high contrast in CL maps (Figs. 1a–1j). Raman spectroscopy shows that the position of the ν_3 (SiO_4) band in synthetic crystals systematically increases from 1008 cm^{-1} (pure Zrn) to 1020 cm^{-1} (pure Hfn) (Fig. 1k), equivalent to the results in Grüneberger et al. (2016). The only detected elements in EDS analysis are Zr, Hf, Si, and O (neglecting C from the surface coating), indicating the absence of impurities at levels >1 wt%

Table 2. Summary of compositional and oxygen isotopic properties (relative to V-SMOW) of synthetic Zrn-Hfn crystals

Run ID	Zr# % EDS[a]	Zr# % SIMS[b]	$\delta^{18}O$ ‰ LF-IRMS[c]	$\delta^{18}O$ ‰ SIMS[d]	IMF[e]	Sputter rate µm³/nA/s	Y %[f]
91500	99.43	99.39(2)	9.86(11)[g]	9.86(14)	0	0.50	2.7
Ar1	0	1.04(3)	2.91(29)	–5.62(23)	–8.54(37)	0.60	2.1
Ar2	98.66(8)	98.9(1)	3.39(1)	2.66(20)	–0.73(20)	0.58	2.3
Ar3	41.2(2.2)	43.8(6)	2.65(20)	–2.78(68)	–5.42(71)	0.56	2.4
Ar4	85.8(1.3)	87.0(1.0)	2.47(31)	0.58(38)	–1.89(49)	0.59	2.3
Ar5	92.6(1.0)	93.2(8)	2.97(76)	2.47(1.06)	–0.50(1.30)	0.57	2.5

[a] Uncertainties are 1 standard deviation for n replicates (n: 91500 = 1; Ar1 = 3; Ar2 = 4; Ar3 = 4; Ar4 = 7; Ar5 = 4); Hf in Ar1 below detection.
[b] Uncertainties are 1 standard deviation for n replicates (n: Ar1 = 4; Ar2 = 4; Ar3 = 4; Ar4 = 4; Ar5 = 76).
[c] Uncertainties are 1 standard deviation for n replicates (n: Ar1 = 3; Ar2 = 2; Ar3 = 3; Ar4 = 4; Ar5 = 2).
[d] Relative to 91500 zircon with 1000 × ln α = +1.55; uncertainties as 1 standard deviation for n = 44 (91500) and n = 12 replicates each for Ar1–Ar5.
[e] IMF as 1000 × ln α with α for 91500 reference zircon set at 0.
[f] Y = useful yield for O^-. Density of intermediate Zrn-Hfn was linearly interpolated from end-member densities 4.67 and 6.97 g/cm³.
[g] Literature value (Wiedenbeck et al. 2004).

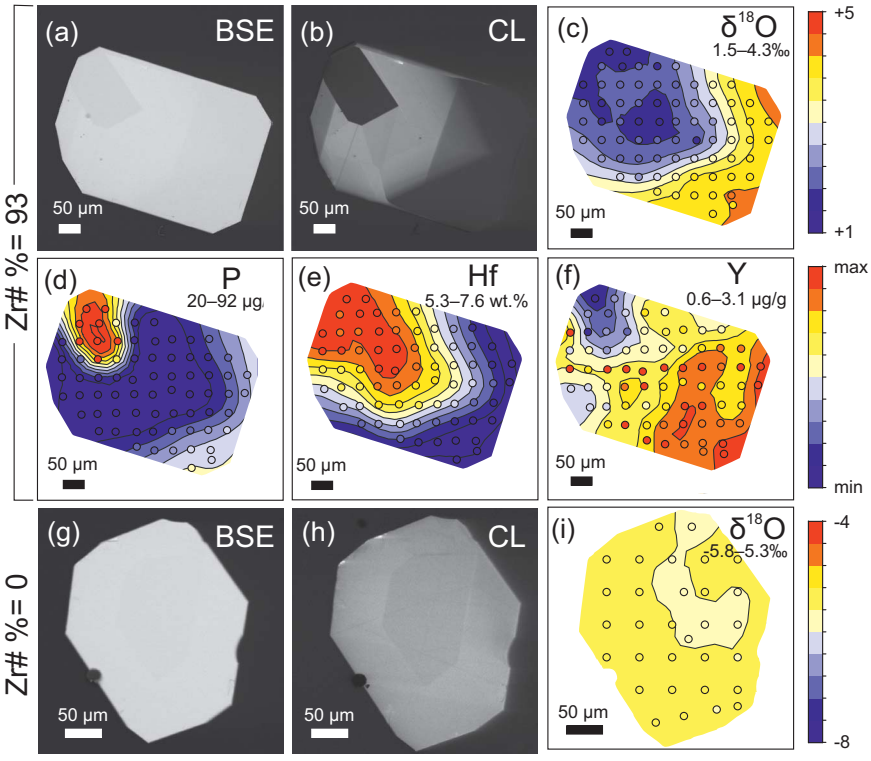

Figure 2. BSE and CL maps along with oxygen isotopic and trace element maps of crystal Ar5–3 (Zr# % = 93; **a**–**f**) and Ar1–1 (Zr# % = 0, hafnon; **g**–**i**). Contouring in 10 intervals was performed in OriginPro 2015 software with the following settings: total point increase factor of 100, smoothing parameter of 0.25, and extrapolation to layer boundaries. For $\delta^{18}O$, the color scale always extends over 4‰ for comparability (**c**, **i**), and it ranges between minimum and maximum values for trace elements (**d**, **e**, **f**).

(Table 2). This was further confirmed by SIMS trace element analyses, where the only trace elements detected at abundances >1 µg/g were P (19–186 µg/g), Y (0.6–19 µg/g), and Lu (0.2–12 µg/g; Online Materials[1] Table S2). Reconnaissance SIMS mass scans for ^{98}Mo further confirmed that synthetic Zrn-Hfn is free from Mo derived from the flux. EDS and SIMS yielded consistent Hf concentrations with relative deviations being on average <18% (Table 2). Values for Zr# are generally close to the targeted end-member compositions, indicating only very minor contributions of Zr in the HfO_2 starting products and vice versa (Table 2).

Trace element mapping of a crystal from run Ar5 (Zr# % = 93; Table 2) shows subtle heterogeneities that correlate with BSE and CL zonation (Fig. 2): a small CL dark domain in the upper left corner of the crystal has high P, whereas the rest except the CL dark domain toward the right and lower right edges of the crystal are comparatively depleted in P (overall range 20–92 µg/g). Although the P-rich domain also has high Hf abundances, the CL-dark domain toward the right and lower right of the crystal (Fig. 2) is depleted in Hf. Yttrium, although present at low abundance between 0.6 and 3.1 µg/g, is anticorrelated with Hf (Pearson correlation coefficient r = –0.60; Fig. 2), but lacks systematic variations with P (r = –0.34).

Synthetic Zrn-Hfn crystals overall range in bulk $\delta^{18}O$ between 2.11‰ and 3.50‰ as determined by LF-IRMS (Online Materials[1] Table S1). Their average $\delta^{18}O$ values (Table 2) are uncorrelated with Zr# (r = 0.25). Replicate analyses show significant heterogeneity as illustrated by crystals from run Ar4, which were analyzed in quadruplicate and range in $\delta^{18}O$ = between 2.11 and 2.85 (Online Materials[1] Table S1). The LF-IRMS analysis of one zircon crystal from run Ar4 yielded $\Delta'^{17}O = -0.101‰$, ~0.05–0.06‰ lower than the terrestrial fractionation line for $\delta^{18}O$ at 2.5‰ (Online Materials[1] Table S1).

SIMS spot analyses of individual crystal domains confirm $\delta^{18}O$ heterogeneity within crystals of the same synthesis run (Table 2): whereas the repeatability of the natural reference zircon 91500 is 0.14 (1 standard deviation; n = 20), higher standard deviations in $\delta^{18}O$ between 0.20 and 1.06 are observed for synthetic zircon crystals (Table 2). The highest standard deviations (0.38–1.06; Table 2) were determined for runs Ar3 to Ar5 with intermediate Zr#. A crystal from run Ar5 (Zr# % = 93) was also mapped in detail for $\delta^{18}O$ variability (Fig. 2c). The overall range in $\delta^{18}O$ (corrected for IMF determined on 91500) is between 1.5 and 4.3‰, with $\delta^{18}O$ and Zr# being highly correlated in this crystal (r = 0.95). By contrast, a crystal from run Arn1 (Zr# % = 0) displays only minor heterogeneity in $\delta^{18}O$ (Fig. 2i).

SIMS oxygen isotopic instrumental mass fractionation in synthetic Zrn-Hfn

Despite the ~1–2‰ heterogeneity in bulk $\delta^{18}O$ between crystals from the same run due to synthesis effects (see Discussion), SIMS analyses of $\delta^{18}O$ and trace elements are co-spatial and thus permit assessing matrix effects at the ~15 µm lateral resolution of individual spots. The $\delta^{18}O$ SIMS averages for synthetic Zrn-Hfn (IMF-corrected using 91500: –5.6‰ to +2.7‰) cover a much larger range than the variability of LF-IRMS values (differences between minimum and maximum raw $\delta^{18}O$ values across all synthetic Zrn-Hfn crystals are 8.3‰ vs. 1.4‰; Table 2). This strongly indicates a compositionally controlled SIMS instrumental isotopic fractionation, which is confirmed by a strong linear correlation

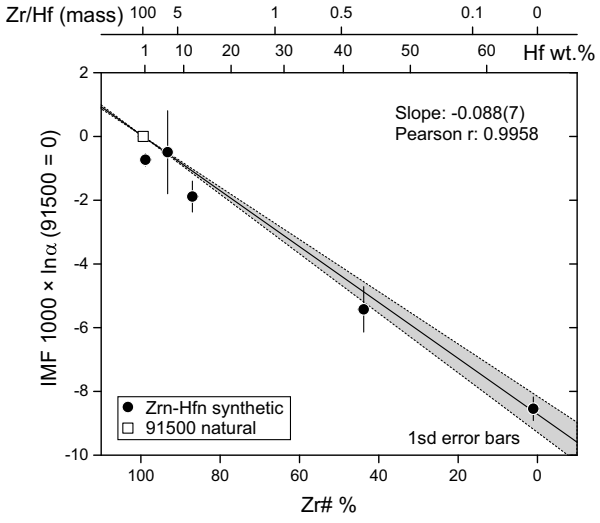

Figure 3. $^{18}O/^{16}O$ instrumental mass fractionation (IMF) against Zr# of synthetic Zrn-Hfn and natural zircon reference 91500; top x-axes show the Hf (wt%) and Zr/Hf (wt) scales for comparison. IMF is expressed as $1000 \times \alpha$ relative to 91500 at zero; normalization was achieved by anchoring the linear regression on the IMF and compositional data for 91500, accounting for uncertainties in X and Y parameters (X errors are within symbol size).

(r = 0.9958) between the IMF values for all synthetic materials against Zr# (Fig. 3). To indicate the isotopic deviation in permil, which would result from a correction of high-Hf zircon when using a low-Hf reference material, the IMF value for 91500 was set to zero (whereas, in fact, the observed IMF value for 91500 varied around $1000 \times \ln \alpha = +1.55$ during the analytical sessions). Linear regression of the data accounting for uncertainties in Zr# and the 91500-normalized IMF as $1000 \times \ln \alpha$ (91500) and forced through 91500 yields the following equation:

$$\text{IMF } 1000 \times \ln \alpha\,(91500) = 0.088(7) \times \text{Zr\#}(\%) - 8.7 \qquad (8)$$

with the slope uncertainty stated as one standard error. For a pure hafnon, this relationship predicts an underdetermination of $\delta^{18}O$ by 8.7‰ (Fig. 3). Volumetric sputter rates for synthetic Zrn-Hfn range between 0.56 and 0.60 μm^3/nA/s, whereas the rate for natural zircon reference 91500 is lower (0.50 μm^3/nA/s; Table 2). Overall, the inverse correlation between Zr# and sputter rate is weak (r = –0.46), but there is a correlation (r = 0.72) between IMF and useful yield Y (the ratio of detected O ions relative to those in the excavated volume), with Y values ranging from 2.1% to 2.7% and the highest value for the natural reference zircon (Table 2).

Discussion

The determination of SIMS IMF values for flux-growth synthetic Zrn-Hfn allows an assessment of the influence of variable Hf abundances in reference and natural zircon on the accuracy of SIMS $\delta^{18}O$ values. Previously, this has only been investigated for high-energy secondary ions (Eiler et al. 1997), which does not apply to current SIMS techniques using multi-collection of low-energy ions in large-geometry instruments (e.g., Isa et al. 2017). Routine $\delta^{18}O$ analysis of zircon using multi-collection

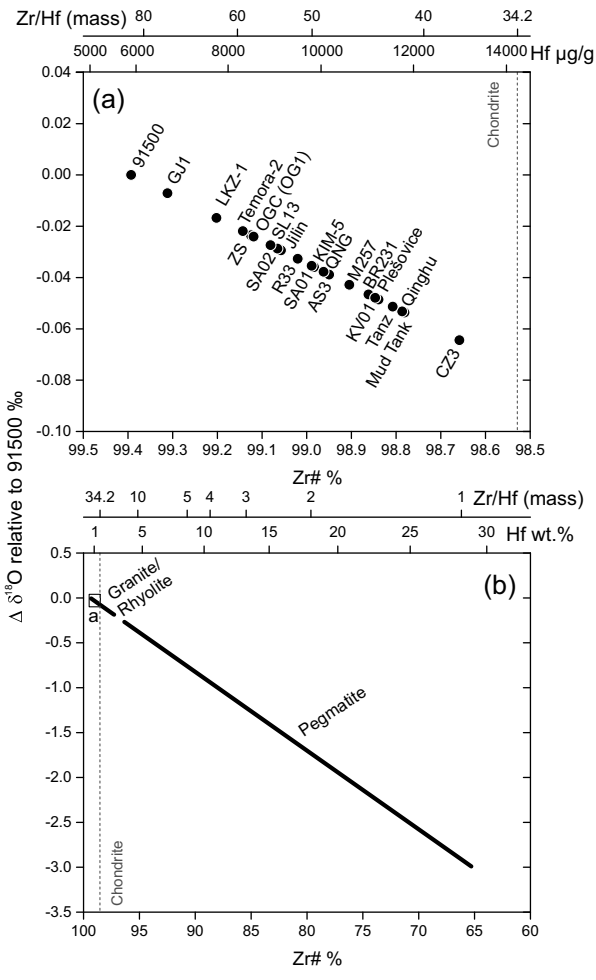

Figure 4. Expected deviation in SIMS zircon $\delta^{18}O$ if 91500 zircon is used as a primary reference to correct for IMF without accounting for a Hf-related matrix effect for (**a**) commonly used reference materials (Table 1), and (**b**) natural zircon from rhyolites/granites and pegmatites (Černý et al. 1985; Lowery Claiborne et al. 2006; Troch et al. 2018; Ayuso et al. 2020). Top x-axes also show the Hf [in µg/g and wt% for (**a**) and (**b**), respectively] and Zr/Hf (wt) scales for comparison.

in large-geometry SIMS instrumentation achieves an in-run analytical precision of ~0.1‰ (1 standard error; Online Materials[1] Table S2). For this, the integration time required from counting statistics, along with the need to average out FC detector noise, is balanced against isotopic fractionation with crater depth. Thus, although longer integration times should theoretically enhance the precision of the isotopic ratio measurement, this will come at the cost of stronger isotopic fractionation with depth, thus potentially resulting in a higher standard error of the mean when ratioing cycle-by-cycle data.

Using Equation 8 (Fig. 3) and compositional data for standard zircon references (averages from 5895–12 980 µg/g, or Zr# % = 98.5–99.5; Table 1), the resulting error without accounting for Hf-compositional variability is at most 0.07‰, and thus inconsequential relative to the in-run analytical uncertainties (Fig. 4a). Zircon reference materials are generally derived from mafic–intermediate igneous rocks (e.g., gabbro,

diorite, syenite), and their Hf-compositional range expectedly overlaps with the lower range of Hf-in-zircon for common granitic-rhyolitic rocks (~8000–26 300 µg/g or Zr# % = 97.3–99.3; e.g., Lowery Claiborne et al. 2006; Troch et al. 2018; Ayuso et al. 2020; Fig. 4b). Only in the most extreme cases as represented by Hf-rich zircon from topaz rhyolite (Congdon and Nash 1991), would an underestimation in $\delta^{18}O$ of –0.4‰ result from an IMF calibration using 91500. Even stronger deviations would occur for analysis of pegmatite zircon: at a maximum of 29 wt% Hf, equivalent to Zr/Hf (mass) = 1 and Zr# % = 66.7 (Černý et al. 1985), the $\delta^{18}O$ value would be ~3‰ too low when calibrated against 91500 zircon reference (Fig. 4b). Oxygen isotopic analysis of pegmatite zircon, which could be useful to identify potential exchange with meteoric waters in commonly radiation-damaged, high-actinide zircon, thus needs to account for matrix effects resulting from Zrn-Hfn solid solution.

Matrix effects for oxygen isotope analysis by SIMS for Zrn-Hfn are comparable in magnitude to those of other solid-solution minerals. However, as with other studies, the exact values vary between instruments and tuning conditions. In contrast to other solid-solution series, the IMF variation along the Zrn-Hfn join is highly linear, whereas, for example, for Fo-Fa, sigmoidal or parabolic functions were used to fit IMF against molar Fe/(Fe+Mg+Mn) (Isa et al. 2017). Similar nonlinear patterns were also observed for Fe/(Fe+Mg+Mn) in carbonates (e.g., Dol-Ank; Fayek et al. 2001; Śliwiński et al. 2016) or Ca/(Ca+Mg+Fe) in garnet (Page et al. 2010; Ickert and Stern 2013). The magnitude of SIMS IMF diminishes with the useful yield, and Isa et al. (2017) argued that the nearly twofold systematically higher volumetric sputtering rate with increasing Fa content in olivine results in a lower steady-state concentration of implanted Cs. Because Cs is a reactive ion species that enhances negative ionization, this in turn may lower secondary ion yields and potentially increase instrumental bias for O isotopes in Fe-rich olivine. Although the differences in volumetric sputtering rates between Zrn and Hfn end-members are only ~6% (and thus barely resolvable; Table 2), the ~9‰ magnitude of the O-isotopic bias for Zrn-Hfn is nearly identical with that for olivine over the full Fo-Fa range (Isa et al. 2017). Thus, although sputter rate may play a role, other structural or compositional properties of the target must also influence ionization yield and the resulting isotopic fractionation. As there is no theoretical model to predict oxygen isotopic fractionation in complex natural materials, we recommend corrections via an empirical linear regression against Zr#, analogous to the practice of IMF corrections for other solid-solution minerals (Fig. 3).

Oxygen isotopic heterogeneity in synthetic Zrn-Hfn is documented in bulk and high spatial resolution analyses. Mapping indicates that coherent domains are isotopically homogeneous at the scale of individual SIMS spots, but that $\delta^{18}O$ heterogeneities of nearly 3‰ exist between domains of the same crystal grown in an intermediate Zr# flux (Fig. 2). These co-vary with Zr# (Fig. 2), but to an extent approximately one order of magnitude larger than expected for a matrix effect caused by differences in Hf abundance (Fig. 4). Compositional and isotopic differences thus appear to have the same origin, rather than the former causing the latter. One possibility for this is that incomplete mixing in the flux produced heterogeneity in $\delta^{18}O$ and Hf concentration, especially as synthetic hafnon (Arn1) is isotopically more homogeneous than crystals synthesized from ZrO_2 and HfO_2 mixtures (Fig. 2). Because partitioning ratios for ^{18}O and ^{16}O are expected to be very close to unity at synthesis temperatures, diffusive fractionation appears unlikely. However, this is difficult to quantify due to poorly known diffusivities in the flux and thicknesses of the crystal-flux boundary layer (Watson and Müller 2009). Exchange of the flux with atmospheric O_2 coupled with local heterogeneities in the flux could also account for some of the observed heterogeneities in the synthetic Zrn-Hfn crystals, as indicated by the (overall minor) heterogeneity of the synthesized end-members. This is supported by three-isotope systematics for synthetic crystals of Ar4, for which $\Delta'^{17}O$ indicates that ~10% of oxygen had exchanged with atmospheric oxygen ($\Delta'^{17}O = –0.5‰$) (Young et al. 2014). This exchange was likely most efficient at the highest temperatures achieved during the synthesis path. The lack of correlation between isotopic composition and position of the analysis spots (i.e., rim locations are not systematically different in $\delta^{18}O$ compared to interiors; Fig. 2) implies that this exchange produced local heterogeneities rather than a wholesale shift in the isotopic composition of the flux over the run duration. We also observe a decoupling between Y and P (Fig. 2), suggesting that the xenotime substitution:

$$2Zr^{4+} \leftrightarrow Y^{3+} + P^{5+} \quad (9)$$

was irrelevant for these synthetic crystals. This also supports local heterogeneities within the flux as the common cause for trace element and isotopic variability in flux-grown Zrn-Hfn crystals.

Implications

Synthetic Zrn-Hfn crystals allow a systematic evaluation of matrix effects for SIMS oxygen isotope analysis. Some oxygen isotopic heterogeneity of these crystals is likely due to incomplete mixing and possibly exchange with atmospheric O_2 during synthesis. Regardless of the minor resulting heterogeneities, results for synthetic Zrn-Hfn crystals indicate that SIMS oxygen isotopic analysis of natural zircon is generally reliable to within ~0.1‰, even when isotopic fractionation resulting from variable Hf abundance is unaccounted for. As Hf is by far the most abundant non-stochiometric component in zircon, matrix effects for oxygen isotopes due to trace components are expected to be similarly minor influences on data accuracy. Zircon crystallized from pegmatitic and other extremely differentiated melts, however, should be scrutinized for potential deviations in SIMS $\delta^{18}O$ determination because of potentially strong differences in Hf abundance between established zircon references and unknowns. Practically, this can be achieved by linear interpolation between the IMF factors determined for the Hfn end-member and other low-Hf zircon reference materials in IMF vs. Zr# space and independently determining Hf in unknown zircon by SIMS or other microanalytical methods.

Acknowledgments and Funding

We thank Boris Burakov and Maria Zamoryanskaya for help with crystal synthesis. Reviewer Chloe Bonamici is thanked for insightful comments, and editor Paul Tomascak for diligent handling of the submission, which improved the presentation. This part of the research was supported by IGEM RAS Research Program #12141500220-0. Aaron Dodd and Martin Danišík are acknowledged for support on the SEM and the optical profilometer, respectively, at the John de Laeter

Centre. The LG-SIMS facility acknowledges funding from AuScope and the Australian Government via the National Collaborative Research Infrastructure Strategy (NCRIS).

References Cited

Aranovich, L.Y. and Bortnikov, N.S. (2018) New Zr–Hf geothermometer for magmatic zircons. Petrology, 26, 115–120, https://doi.org/10.1134/S0869591118020029.

Ávila, J.N., Ireland, T.R., Holden, P., Lanc, P., Latimore, A., Schram, N., Foster, J., Williams, I.S., Loiselle, L., and Fu, B. (2020) High-precision, high-accuracy oxygen isotope measurements of Zircon reference materials with the SHRIMP-SI. Geostandards and Geoanalytical Research, 44, 85–102, https://doi.org/10.1111/ggr.12298.

Ayuso, R.A., Foley, N.K., Vazquez, J.A., and Jackson, J.C. (2020) SHRIMP U-Pb zircon geochronology of volcanic rocks hosting world class Be-U mineralization at Spor Mountain, Utah, USA. Journal of Geochemical Exploration, 209, 106401, https://doi.org/10.1016/j.gexplo.2019.106401.

Baertschi, P. (1976) Absolute ^{18}O content of standard mean ocean water. Earth and Planetary Science Letters, 31, 341–344, https://doi.org/10.1016/0012-821X(76)90115-1.

Bau, M. (1996) Controls on the fractionation of isovalent trace elements in magmatic and aqueous systems: Evidence from Y/Ho, Zr/Hf, and lanthanide tetrad effect. Contributions to Mineralogy and Petrology, 123, 323–333, https://doi.org/10.1007/s004100050159.

Bindeman, I.N. and Melnik, O.E. (2022) The rises and falls of zirconium isotopes during zircon crystallisation. Geochemical Perspectives Letters, 24, 17–21, https://doi.org/10.7185/geochemlet.2241.

Black, L.P., Kamo, S.L., Allen, C.M., Davis, D.W., Aleinikoff, J.N., Valley, J.W., Mundil, R., Campbell, I.H., Korsch, R.J., Williams, I.S., and others. (2004) Improved $^{206}Pb/^{238}U$ microprobe geochronology by the monitoring of a trace-element-related matrix effect; SHRIMP, ID-TIMS, ELA-ICP-MS and oxygen isotope documentation for a series of zircon standards. Chemical Geology, 205, 115–140, https://doi.org/10.1016/j.chemgeo.2004.01.003.

Booth, A.L., Kolodny, Y., Chamberlain, C.P., McWilliams, M., Schmitt, A.K., and Wooden, J. (2005) Oxygen isotopic composition and U-Pb discordance in zircon. Geochimica et Cosmochimica Acta, 69, 4895–4905, https://doi.org/10.1016/j.gca.2005.05.013.

Cavosie, A.J., Valley, J.W., Kita, N.T., Spicuzza, M.J., Ushikubo, T., and Wilde, S.A. (2011) The origin of high $\delta^{18}O$ zircons: Marbles, megacrysts, and metamorphism. Contributions to Mineralogy and Petrology, 162, 961–974, https://doi.org/10.1007/s00410-011-0634-3.

Černý, P., Meintzer, R.E., and Anderson, A.J. (1985) Extreme fractionation in rare-element granitic pegmatites; selected examples of data and mechanisms. Canadian Mineralogist, 23, 381–421.

Cheong, A.C., Jeong, Y.-J., Lee, S., Yi, K., Jo, H.J., Lee, H.-S., Park, C., Kim, N.K., Li, X.-H., and Kamo, S.L. (2019) LKZ-1: A new zircon working standard for the in situ determination of U-Pb age, O-Hf isotopes, and trace element composition. Minerals, 9, 325, https://doi.org/10.3390/min9050325.

Cherniak, D.J., Hanchar, J.M., and Watson, E.B. (1997) Diffusion of tetravalent cations in zircon. Contributions to Mineralogy and Petrology, 127, 383–390, https://doi.org/10.1007/s004100050287.

Coble, M.A., Vazquez, J.A., Barth, A.P., Wooden, J., Burns, D., Kylander-Clark, A., Jackson, S., and Vennari, C.E. (2018) Trace element characterisation of MAD-559 zircon reference material for ion microprobe analysis. Geostandards and Geoanalytical Research, 42, 481–497, https://doi.org/10.1111/ggr.12238.

Congdon, R.D. and Nash, W.P. (1991) Eruptive pegmatite magma: Rhyolite of the Honeycomb Hills, Utah. American Mineralogist, 76, 1261–1278.

Coogan, L.A., Manning, C.E., and Wilson, R.N., and the E.I.M.F. (2007) Oxygen isotope evidence for short-lived high-temperature fluid flow in the lower oceanic crust at fast-spreading ridges. Earth and Planetary Science Letters, 260, 524–536, https://doi.org/10.1016/j.epsl.2007.06.013.

Eiler, J.M., Graham, C., and Valley, J.W. (1997) SIMS analysis of oxygen isotopes: Matrix effects in complex minerals and glasses. Chemical Geology, 138, 221–244, https://doi.org/10.1016/S0009-2541(97)00015-6.

Fayek, M., Harrison, T.M., Grove, M., McKeegan, K.D., Coath, C.D., and Boles, J.R. (2001) In situ stable isotopic evidence for protracted and complex carbonate cementation in a petroleum reservoir, North Coles Levee, San Joaquin Basin, California, USA. Journal of Sedimentary Research, 71, 444–458, https://doi.org/10.1306/2DC40954-0E47-11D7-8643000102C1865D.

Finch, R.J. and Hanchar, J.M. (2003) Structure and chemistry of zircon and zircon-group minerals. Reviews in Mineralogy and Geochemistry, 53, 1–25, https://doi.org/10.2113/0530001.

Gain, S.E., Gréau, Y., Henry, H., Belousova, E., Dainis, I., Griffin, W.L., and O'Reilly, S.Y. (2019) Mud Tank Zircon: Long-term evaluation of a reference material for U-Pb dating, Hf-isotope analysis and trace element analysis. Geostandards and Geoanalytical Research, 43, 339–354, https://doi.org/10.1111/ggr.12265.

Grüneberger, A.M., Schmidt, C., Jahn, S., Rhede, D., Loges, A., and Wilke, M. (2016) Interpretation of Raman spectra of the zircon-hafnon solid solution. European Journal of Mineralogy, 28, 721–733, https://doi.org/10.1127/ejm/2016/0028-2551.

Hanchar, J.M., Finch, R.J., Hoskin, P.W.O., Watson, E.B., Cherniak, D.J., and Mariano, A.N. (2001) Rare earth elements in synthetic zircon: Part 1. Synthesis, and rare earth element and phosphorus doping. American Mineralogist, 86, 667–680, https://doi.org/10.2138/am-2001-5-607.

Hanchar, J.M., Burakov, B.E., Anderson, E.B., and Zamoryanskaya, M.V. (2002) Investigation of single crystal zircon, $(Zr,Pu)SiO_4$, doped with ^{238}Pu. Proceedings of the Materials Research Society, 757, 215–225, https://doi.org/10.1557/PROC-757-II6.9.

Härtel, B., Jonckheere, R., Wauschkuhn, B., Hofmann, M., Frölich, S., and Ratschbacher, L. (2021) Zircon Raman dating: Age equation and calibration. Chemical Geology, 579, 120351, https://doi.org/10.1016/j.chemgeo.2021.120351.

Hawkesworth, C.J. and Kemp, A.I.S. (2006) Using hafnium and oxygen isotopes in zircons to unravel the record of crustal evolution. Chemical Geology, 226, 144–162, https://doi.org/10.1016/j.chemgeo.2005.09.018.

Hu, Z., Li, X.-H., Luo, T., Zhang, W., Crowley, J., Li, Q., Ling, X., Yang, C., Li, Y., Feng, L., and others. (2021) Tanz zircon megacrysts: A new zircon reference material for the microbeam determination of U-Pb ages and Zr-O isotopes. Journal of Analytical Atomic Spectrometry, 36, 2715–2734, https://doi.org/10.1039/D1JA00311A.

Huang, C., Wang, H., Yang, J.H., Ramezani, J., Yang, C., Zhang, S.B., Yang, Y.H., Xia, X.P., Feng, L.J., Lin, J., and others. (2020) SA01-A proposed zircon reference material for microbeam U-Pb age and Hf-O isotopic determination. Geostandards and Geoanalytical Research, 44, 103–123, https://doi.org/10.1111/ggr.12307.

Huang, C., Wang, H., Yang, J., Yang, C., Li, Z., Yang, Y., Feng, L., Xie, L., and Wu, S. (2021) Characterization of the potential reference material SA02 for micro-beam U-Pb geochronology and Hf-O isotopic composition analysis of zircon. Journal of Analytical Atomic Spectrometry, 36, 368–374, https://doi.org/10.1039/D0JA00409J.

Ickert, R.B. and Stern, R.A. (2013) Matrix Corrections and Error Analysis in High-Precision SIMS $^{18O/16}O$ Measurements of Ca-Mg-Fe Garnet. Geostandards and Geoanalytical Research, 37, 429–448, https://doi.org/10.1111/j.1751-908X.2013.00222.x.

Isa, J., Kohl, I.E. , Liu, M.C., Wasson, J.T., Young, E.D., and McKeegan, K.D. (2017) Quantification of oxygen isotope SIMS matrix effects in olivine samples: Correlation with sputter rate. Chemical Geology, 458, 14–21, https://doi.org/10.1016/j.chemgeo.2017.03.020.

Kooymans, C., Magee, C.W. Jr., Waltenberg, K., Evans, N.J., Bodorkos, S., Amelin, Y., Kamo, S.L., and Ireland, T. (2024) Effect of chemical abrasion of zircon on SIMS U-Pb, $\delta^{18}O$, trace element, and LA-ICPMS trace element and Lu-Hf isotopic analyses. Geochronology, 6, 337–363, https://doi.org/10.5194/gchron-6-337-2024.

Lackey, J.S., Valley, J.W., and Saleeby, J.B. (2005) Supracrustal input to magmas in the deep crust of Sierra Nevada batholith: Evidence from high-$\delta^{18}O$ zircon. Earth and Planetary Science Letters, 235, 315–330, https://doi.org/10.1016/j.epsl.2005.04.003.

Li, X., Tang, G., Gong, B., Yang, Y., Hou, K., Hu, Z., Li, Q., Liu, Y., and Li, W. (2013) Qinghu zircon: A working reference for microbeam analysis of U-Pb age and Hf and O isotopes. Chinese Science Bulletin, 58, 4647–4654, https://doi.org/10.1007/s11434-013-5932-x.

Liebmann, J., Spencer, C.J., Kirkland, C.L., Xia, X.P., and Bourdet, J. (2021) Effect of water on $\delta^{18}O$ in zircon. Chemical Geology, 574, 120243, https://doi.org/10.1016/j.chemgeo.2021.120243.

Liebmann, J., Kirkland, C.L., Cliff, J.B., Spencer, C.J., and Cavosie, A.J. (2023) Strategies towards robust interpretations of in situ zircon oxygen isotopes. Geoscience Frontiers, 14, 101523, https://doi.org/10.1016/j.gsf.2022.101523.

Ling, X.-X., Li, Q.-L., Yang, C., Chu, Z.-Y., Feng, L.-J., Huang, C., Huang, L.-L., Zhang, H., Hou, Z.-H., and Xu, J.-J. (2022) Zircon ZS—A homogenous natural reference material for U-Pb age and O-Hf isotope microanalyses. Atomic Spectroscopy, 43, 134–144, https://doi.org/10.46770/AS.2022.033.

Lowery Claiborne, L., Miller, C.F., Walker, B.A., Wooden, J.L., Mazdab, F.K., and Bea, F. (2006) Tracking magmatic processes through Zr/Hf ratios in rocks and Hf and Ti zoning in zircons: An example from the Spirit Mountain batholith, Nevada. Mineralogical Magazine, 70, 517–543, https://doi.org/10.1180/0026461067050348.

Luo, T., Li, Q., Ling, X., Li, Y., Yang, C., Wang, H., Xia, X., Zhang, S., Xu, L., Liu, X., and others. (2021) Jilin zircon–a new natural reference material for microbeam U-Pb geochronology and Hf-O isotopic analysis. Journal of Analytical Atomic Spectrometry, 36, 2216–2226, https://doi.org/10.1039/D1JA00258A.

Nasdala, L., Hofmeister, W., Norberg, N., Martinson, J.M., Corfu, F., Dörr, W., Kamo, S.L., Kennedy, A.K., Kronz, A., Reiners, P.W., and others. (2008) Zircon M257-a homogeneous natural reference material for the ion microprobe U-Pb analysis of zircon. Geostandards and Geoanalytical Research, 32, 247–265, https://doi.org/10.1111/j.1751-908X.2008.00914.x.

Neumann, A., Kahlenberg, V., Lerche, I., Stöber, S., and Pöllmann, H. (2024) Synthesis and Characterization of Single Crystal Zircon-Hafnon $Zr_{(1-x)}Hf_{(x)}SiO_4$ Solid Solutions and the Comparison with the Reaction Products of a TEOS-Based Hydrothermal Route. ACS Omega, 9, 15781–15803, https://doi.org/10.1021/acsomega.3c06960.

Page, F.Z., Fu, B., Kita, N.T., Fournelle, J., Spicuzza, M.J., Schulze, D.J., Viljoen, F., Basei, M.A., and Valley, J.W. (2007) Zircons from kimberlite: New insights from oxygen isotopes, trace elements, and Ti in zircon thermometry. Geochimica et Cosmochimica Acta, 71, 3887–3903, https://doi.org/10.1016/j.gca.2007.04.031.

Page, F.Z., Kita, N.T., and Valley, J.W. (2010) Ion microprobe analysis of oxygen isotopes in garnets of complex chemistry. Chemical Geology, 270, 9–19, https://doi.org/10.1016/j.chemgeo.2009.11.001.

Pearce, N.J., Perkins, W.T., Westgate, J.A., Gorton, M.P., Jackson, S.E., Neal, C.R., and Chenery, S.P. (1997) A compilation of new and published major and trace element data for NIST SRM 610 and NIST SRM 612 glass reference materials. Geostandards Newsletter, 21, 115–144, https://doi.org/10.1111/j.1751-908X.1997.tb00538.x.

Petersson, A., Kemp, A.I., Hickman, A.H., Whitehouse, M.J., Martin, L., and Gray, C.M. (2019) A new 3.59 Ga magmatic suite and a chondritic source to the east Pilbara Craton. Chemical Geology, 511, 51–70, https://doi.org/10.1016/j.chemgeo.2019.01.021.

Piazolo, S., Belousova, E., La Fontaine, A., Corcoran, C., and Cairney, J.M. (2017) Trace element homogeneity from micron-to atomic scale: Implication for the suitability of the zircon GJ-1 as a trace element reference material. Chemical Geology, 456, 10–18, https://doi.org/10.1016/j.chemgeo.2017.03.001.

Sláma, J., Košler, J., Condon, D.J., Crowley, J.L., Gerdes, A., Hanchar, J.M., Horstwood, M.S., Morris, G.A., Nasdala, L., Norberg, N., and others. (2008) Plešovice zircon—A new natural reference material for U–Pb and Hf isotopic microanalysis. Chemical Geology, 249, 1–35, https://doi.org/10.1016/j.chemgeo.2007.11.005.

Śliwiński, M.G., Kitajima, K., Kozdon, R., Spicuzza, M.J., Fournelle, J.H., Denny, A., and Valley, J.W. (2016) Secondary ion mass spectrometry bias on isotope ratios in dolomite–ankerite, Part I: $\Delta^{18}O$ matrix effects. Geostandards and Geoanalytical Research, 40, 157–172, https://doi.org/10.1111/j.1751-908X.2015.00364.x.

Tompkins, H.G., Zieman, L.J., Ibanez-Mejia, M., and Tissot, F.L. (2020) Zirconium stable isotope analysis of zircon by MC-ICP-MS: Methods and application to evaluating intra-crystalline zonation in a zircon megacryst. Journal of Analytical Atomic Spectrometry, 35, 1167–1186, https://doi.org/10.1039/C9JA00315K.

Trail, D., Mojzsis, S.J., Harrison, T.M., Schmitt, A.K., Watson, E.B., and Young, E.D. (2007) Constraints on Hadean zircon protoliths from oxygen isotopes, Ti-thermometry, and rare earth elements. Geochemistry, Geophysics, Geosystems, 8, 2006GC001449, https://doi.org/10.1029/2006GC001449.

Trail, D., Boehnke, P., Savage, P.S., Liu, M.C., Miller, M.L., and Bindeman, I. (2018) Origin and significance of Si and O isotope heterogeneities in Phanerozoic, Archean, and Hadean zircon. Proceedings of the National Academy of Sciences of the United States of America, 115, 10287–10292, https://doi.org/10.1073/pnas.1808335115.

Troch, J., Ellis, B.S., Schmitt, A.K., Bouvier, A.S., and Bachmann, O. (2018) The dark side of zircon: Textural, age, oxygen isotopic and trace element evidence of fluid saturation in the subvolcanic reservoir of the Island Park-Mount Jackson Rhyolite, Yellowstone (USA). Contributions to Mineralogy and Petrology, 173, 54, https://doi.org/10.1007/s00410-018-1481-2.

Valley, J.W. (2003) Oxygen isotopes in zircon. Reviews in Mineralogy and Geochemistry, 53, 343–385, https://doi.org/10.2113/0530343.

Watson, E.B. and Müller, T. (2009) Non-equilibrium isotopic and elemental fractionation during diffusion-controlled crystal growth under static and dynamic conditions. Chemical Geology, 267, 111–124, https://doi.org/10.1016/j.chemgeo.2008.10.036.

Wei, Q., Wang, H., Yang, Y., Yang, J., Huang, C., Wu, S., and Xie, L. (2020) KV01 zircon—A potential New Archean reference material for microbeam U-Pb age and Hf-O isotope determinations. Science China. Earth Sciences, 63, 1780–1790, https://doi.org/10.1007/s11430-019-9638-y.

Weyer, S., Münker, C., Rehkämper, M., and Mezger, K. (2002) Determination of ultra-low Nb, Ta, Zr and Hf concentrations and the chondritic Zr/Hf and Nb/Ta ratios by isotope dilution analyses with multiple collector ICP-MS. Chemical Geology, 187, 295–313, https://doi.org/10.1016/S0009-2541(02)00129-8.

Whattam, J., Sharpe, R., Skelton, S., Day, M.C., Fayek, M., and Hawthorne, F.C. (2022) Mass bias corrections for hydrogen and oxygen isotope analysis of tourmaline by secondary ion mass spectrometry. Canadian Mineralogist, 60, 775–786, https://doi.org/10.3749/canmin.2200005.

Wiedenbeck, M., Alle, P., Corfu, F., Griffin, W.L., Meier, M., Oberli, F., Quadt, A., Roddick, J., and Spiegel, W. (1995) Three natural zircon standards for U-Th-Pb, Lu-Hf, trace element and REE analyses. Geostandards Newsletter, 19, 1–23, https://doi.org/10.1111/j.1751-908X.1995.tb00147.x.

Wiedenbeck, M., Hanchar, J.M., Peck, W.H., Sylvester, P., Valley, J., Whitehouse, M., Kronz, A., Morishita, Y., Nasdala, L., Fiebig, J., and others. (2004) Further characterisation of the 91500 zircon crystal. Geostandards and Geoanalytical Research, 28, 9–39, https://doi.org/10.1111/j.1751-908X.2004.tb01041.x.

Wotzlaw, J.F., Bindeman, I.N., Schaltegger, U., Brooks, C.K., and Naslund, H.R. (2012) High-resolution insights into episodes of crystallization, hydrothermal alteration and remelting in the Skaergaard intrusive complex. Earth and Planetary Science Letters, 355-356, 199–212, https://doi.org/10.1016/j.epsl.2012.08.043.

Xia, X.-P., Cui, Z.-X., Li, W., Zhang, W.-F., Yang, Q., Hui, H., and Lai, C.-K. (2019) Zircon water content: Reference material development and simultaneous measurement of oxygen isotopes by SIMS. Journal of Analytical Atomic Spectrometry, 34, 1088–1097, https://doi.org/10.1039/C9JA00073A.

Young, E.D., Yeung, L.Y., and Kohl, I.E. (2014) On the $\Delta^{17}O$ budget of atmospheric O_2. Geochimica et Cosmochimica Acta, 135, 102–125, https://doi.org/10.1016/j.gca.2014.03.026.

Yui, T.F., Rumble, D. III, Chen, C.H., and Lo, C.H. (1997) Stable isotope characteristics of eclogites from the ultra-high-pressure metamorphic terrain, east-central China. Chemical Geology, 137, 135–147, https://doi.org/10.1016/S0009-2541(96)00153-2.

Manuscript received May 9, 2025
Manuscript accepted July 27, 2025
Accepted manuscript online August 7, 2025
Manuscript Handled by Paul Tomascak

Endnotes:

[1]Deposit item AM-25-129886. Online Materials are free to all readers. Go online, via the table of contents or article view, and find the tab or link for supplemental materials.